

Efficient Network Construction through Structural Plasticity

Xiaocong Du, *Student Member, IEEE*, Zheng Li, *Student Member, IEEE*, Yufei Ma, *Member, IEEE*,
and Yu Cao, *Fellow, IEEE*

Abstract—Deep Neural Networks (DNNs) on hardware is facing excessive computation cost due to the massive number of parameters. A typical training pipeline to mitigate over-parameterization is to pre-define a DNN structure first with redundant learning units (filters and neurons) under the goal of high accuracy, then to prune redundant learning units after training with the purpose of efficient inference. We argue that it is sub-optimal to introduce redundancy into training for the purpose of reducing redundancy later in inference. Moreover, the fixed network structure further results in poor adaption to dynamic tasks, such as lifelong learning. In contrast, structural plasticity plays an indispensable role in mammalian brains to achieve compact and accurate learning. Throughout the lifetime, active connections are continuously created while those are no longer important are degenerated. Inspired by such observation, we propose a training scheme, namely Continuous Growth and Pruning (CGaP), where we start the training from a small network seed, then literally execute continuous growth by adding important learning units and finally prune secondary ones for efficient inference. The inference model generated from CGaP is sparse in the structure, largely decreasing the inference power and latency when deployed on hardware platforms. With popular DNN structures on representative datasets, the efficacy of CGaP is benchmarked by both algorithm simulation and architectural modeling on Field-programmable Gate Arrays (FPGA). For example, CGaP decreases the FLOPs, model size, DRAM access energy and inference latency by 63.3%, 64.0%, 11.8% and 40.2%, respectively, for ResNet-110 on CIFAR-10.

Index Terms—Deep learning, structural plasticity, model pruning, hardware acceleration, algorithm-hardware co-design.

I. INTRODUCTION

DEEP Neural Networks have various applications including image classification [1], object detection [2], speech recognition [3] and natural language processing [4]. However, the accuracy of DNNs is heavily relies on massive amounts of parameters and deep structures, making it hard to deploy DNNs on resource-limited embedded systems. When training or inferring the DNN models on hardware, the model must be stored in the external memory such as dynamic random-access memory (DRAM) and fetched multiple times. These operations are expensive in computation, memory access and energy consumption. For example, Fig. 1 shows the energy consumption of one inference pass in several modern DNN

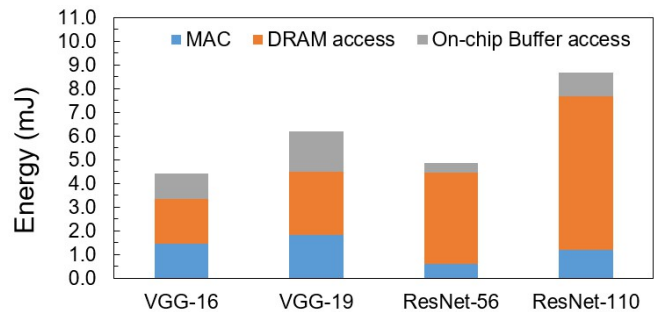


Fig. 1: Energy breakdown for modern DNN structures, results from simulation by the FPGA performance model [5]. Due to the redundancy in parameters, multiply-accumulator (MAC) and external memory (DRAM) access dominate the energy consumption.

structures, simulated by the FPGA performance model [5] under the setting of 300 MHz operating frequency and 19.2 GB/s DRAM bandwidth. The input image size is 32×32 . A typical DNN model is too large to fit in on-chip memory. For instance, VGG-19 [6] has 20.4M parameters. Running such a model requires frequent external memory access, exacerbating the power consumption of a typical embedded system.

Previous researches have designed customized hardware for DNN acceleration [7], [8], but limited to relatively small neural networks, such as LeNet-5 [9]. Other works focused on data reuse of convolutional layers and demonstrated the results on specific hardware [7], [10], [11], [12]. However, their improvement is limited on those networks where fully connected layer is widely used, such as RNNs and LSTMs.

To support more general network models, network pruning is a popular approach by removing secondary weights and neurons. Network pruning executes a three-step procedure which trains a pre-designed network from scratch, removes less important connections or filters/neurons according to a saliency score (a metrics to measure the importance of weights and learning units) [13], [14], [15], [16], [17], or by adding a regularization term into the loss function [18], [19], and finally fine-tune.

However, the above pruning techniques suffer from two limitations: (1) training a large and fixed network from scratch could be sub-optimal as it introduces redundancy; (2) in the process of training, pruning only discards less important weights at the end of training but does not strengthens important weights and nodes. These limitations of network pruning confine the learning performance as well as the model pruning

Xiaocong Du, Yufei Ma and Yu Cao are with the School of Electrical, Computer and Energy Engineering, Arizona State University, Tempe, AZ 85287, USA (e-mail: xiaocong@asu.edu; yufeima@asu.edu; ycao@asu.edu).

Zheng Li is with the School of Computing, Informatics, and Decision Systems Engineering, Arizona State University, Tempe, AZ 85287, USA (e-mail: zhengl11@asu.edu).

Preprint. Under review.

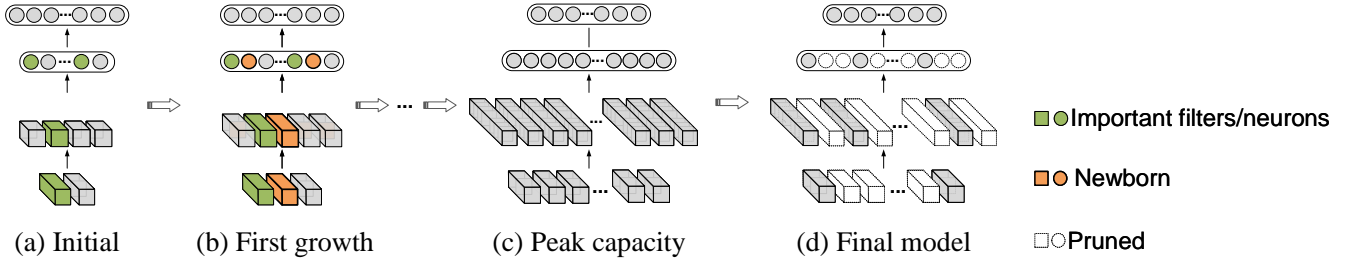


Fig. 2: The proposed CGaP scheme. CGaP starts the training from a seed network instead of an over-parameterized one, gradually grows important learning units during the training and reaches peak capacity at the end of growth, then prunes secondary filters and neurons to generate an inference model with structured sparsity and up-to-date accuracy.

efficiency (i.e., how many parameters can be removed and how structured the sparsity is).

In contrast to the static DNN model in training, the biological nervous system exhibits active growth and pruning through the lifetime. [20], [21], [22] have observed that rapid growth of neurons and synapses takes place in an infant’s brain and is vital to the maturity of an adult’s brain. In brains, some neurons and synapses are used more frequently and are consequently strengthened. Those neurons and synapses that are not used consistently are weakened and removed. This structural plasticity of the brain is central to the study of developmental biology.

Inspired by this observation from biology, we propose a training scheme named Continuous Growth and Pruning (CGaP), which leverages structural plasticity to tackle the aforementioned limitations of pruning techniques. Instead of training an over-parameterized network from scratch, CGaP starts the training from a small network seed (Fig. 2(a)), whose size is as low as 0.1%-3% of the full-size reference model. In each iteration of the growth, CGaP locally sorts neurons and filters (also known as output channels in some literature) according to our saliency score (Section III-B). Based on the saliency score, important learning units are selected and corresponding new units are added in (Fig. 2(b)). The selection and expansion of important units help reinforce the purpose of learning and increase model capacity. A filter-wise and neuron-wise pruning will then execute on the post-growth model (Fig. 2(c)) based on pruning metrics. CGaP generates a significantly sparse and structured inference model (Fig. 2(d)) with accuracy improvement. In the generated inference model, a large amount of filters and neurons are removed. Compared to non-structured pruning [13], CGaP benefits hardware implementation as it reduces the computation volume and memory access without additional hardware architecture changes.

Algorithmic experiments and hardware simulations validate that CGaP significantly decreases the number of external and on-chip memory accesses, and accelerates the inference by bypassing the removed filters and neurons. On the algorithm side, we demonstrate the performance in accuracy and model pruning on several networks and datasets. For instance, CGaP reduces 78.9% parameters of VGG-19 with +0.37% accuracy improvement on CIFAR-100, 85.8% parameters with +0.23% accuracy improvement on SVHN [23]. For ResNet-110 [24], CGaP reduces 64.0% parameters with +0.09% accuracy im-

provement on CIFAR-10. These results exceed the state-of-the-art pruning methods [13], [14], [15], [16], [25], [26]. Furthermore, we validate the efficiency of the inference model generated from CGaP on a FPGA simulator [5]. For one inference pass of VGG-19 on CIFAR-100 [27], previous non-structured pruning approach [13] requires energy consumption of 2.7×10^9 pJ in accessing DRAM and 5.6 ms inference latency, while CGaP requires only 2.2×10^9 pJ and 4.4 ms latency.

The contribution of this paper is as follows:

- A brain-inspired training flow (CGaP) with a dynamic structure is proposed. CGaP grows the network from a small seed and effectively reduces over-parameterization without sacrificing the accuracy.
- The advantage of structured sparsity of the inference model generated from CGaP is validated on a high-level FPGA performance model from the perspective of on-chip buffer access energy, external memory access energy and inference latency.
- The discussion and understanding on why the growth improves the learning efficiency.

The rest of the paper is organized as follows. Section II introduces the background of model pruning. Section III demonstrates the saliency score used to select the learning units. Section IV describes the proposed Continuous Growth and Pruning scheme. Section V presents the experimental results from algorithmic simulations. Section VI demonstrates the simulation results from FPGA performance modeling. Section VII discusses the understanding of network plasticity as well as ablation study. Section VIII concludes this work and discusses the insight into future work.

II. PREVIOUS WORK

There has been broad interest in reducing the redundancy of DNNs in order to deploy them on a resource-limited hardware platform. The structural surgery is a widely used approach and can be categorized into a destructive direction and a constructive direction. We will discuss the related work, as well as orthogonal approaches to our methods in this section.

A. Destructive Methods

Destructive methods zero out specific connections or remove filters in convolutional layers, and neurons in fully-

connected layers, generating a sparse model. Weight magnitude pruning [13] pruned weights by setting the selected weight to be zero. The selection is based on L1-norm, i.e., the absolute value of the weight. Weight magnitude pruning generates a sparse weight matrix, but not in a structured way. In this case, specific hardware design [28] is needed to take advantage of the optimized inference model; otherwise, the non-structured sparsity does not benefit hardware acceleration due to the overhead in model management. The kernel-wise pruning [14] pruned kernels layer by layer based on the saliency metrics of each filter and achieved structured sparsity in the inference model. Compared to [14], CGaP prunes filters, leading to more structured inference model. Besides the saliency-based pruning, the penalty-based approach has been explored by [19], [29] and structured sparsity was achieved. Our method is different from all the above pruning schemes from two perspectives: (1) We start training from a small seed other than an over-parameterized network; (2) Besides removing secondary filters/neurons, we also reinforce important ones to further improve learning accuracy and model compactness.

B. Constructive Methods

Constructive approaches include techniques that add new connections or filters to enlarge the model capacity. [30], [31] increased network size by adding random neurons with fresh initialization (i.e, weights are randomly initialized, without pre-trained information). They evaluated their approach on basic XOR problems. Different from their approach, CGaP selectively adds neurons and filters that are initialized with the information learned in the previous training. Meanwhile, CGaP is validated on modern DNNs and datasets from a more realistic scenario. [32] constructed the DNN by activating connections and choosing a set of convolutional filters among a bunch of random filters according to their influence on the training performance. However, this approach highly depended on trials and errors to find the optimal set of filters that reduce the most loss. This approach is sensitive to power and timing budgets, limiting its extension on large datasets. Unlike their work, CGaP directly grows the network from a seed, minimizing the effort on trails and errors.

C. Orthogonal Methods

Orthogonal methods, such as low-precision quantization and low-rank decomposition, compress the DNN model by quantizing the parameters to fewer bits [33], [34], or by finding a low-rank approximation [35], [36]. Note that our CGaP approach can be combined with these orthogonal methods to further improve inference efficiency.

III. SALIENCY SCORE

In this section, we describe the detailed methodology of CGaP, starting from the saliency score to sample of the importance of a learning unit. Section III-A defines the terminology we use in this paper. Section III-B provides the mathematical proof of the saliency score we adopt.

A. Terminology

A DNN can be treated as a feedforward multi-layer architecture that maps the input images to certain output vectors. Each layer is a certain function, such as convolution, ReLU, pooling and inner product, whose input is \mathcal{X} , output is \mathcal{Y} and the parameter is \mathcal{W} in case of convolutional and fully connected layers. Hereby the convolutional layer (conv-layer) is formulated as: $\mathcal{Y}_l = \mathcal{X}_l * \mathcal{W}_l$, wherein $\mathcal{X}_l \in \mathbb{R}^{I_l \times W_{l_i} \times H_{l_i}}$, $\mathcal{Y}_l \in \mathbb{R}^{O_l \times W_{o_l} \times H_{o_l}} \Leftrightarrow \mathcal{X}_{l+1} \in \mathbb{R}^{I_{l+1} \times W_{l+1} \times H_{l+1}}$, $\mathcal{W}_l \in \mathbb{R}^{O_l \times I_l \times K \times K}$, where subscript l denotes index of layer. And the fully connected layer is represented by: $\mathcal{Y}_l = \mathcal{X}_l \cdot \mathcal{W}_l$, where the input $\mathcal{X}_l \in \mathbb{R}^{I_l}$, the output $\mathcal{Y}_l \in \mathbb{R}^{O_l} \Leftrightarrow \mathcal{X}_{l+1} \in \mathbb{R}^{I_{l+1}}$, and the parameter matrix is $\mathcal{W}_l \in \mathbb{R}^{O_l, I_l}$.

a) *Convolutional layer (conv-layer) l* : the 4 dimensions of its weight matrix are: the number of output channel O_l , number of input channel I_l , kernel width and height K respectively. We denote the o -th 3D **filter** which generates the o -th output channel in the feature map as $W_l^o \in \mathbb{R}^{I_l \times K \times K}$, the i -th 2D **kernel** in the o -th filter is $W_l^{o,i} \in \mathbb{R}^{K \times K}$. On the other hand, a 4D weight tensor $W_l^i \in \mathbb{R}^{O_l \times 1 \times K \times K}$ is a package of O_l kernels across all output channels at the i -th input channel. For example, in Fig. 3, $W_{l,picked}^j$ is a 3D filter consists of I_l kernels; $W_{l+1,projected}^j$ and $W_{l+1,mapped}^j$ are both **4D tensor** across all output channels. The $W_l^{o,i,m,n} \in \mathbb{R}^{1 \times 1}$ refers to the weight pixel at the cross of the m -th row and the n -th column in the kernel which locates in the o -th filter at the i -th input channel.

b) *Fully-connected layer (fc-layer) l* : input \mathcal{X}_l propagate from one hidden activation i to the next layer. We refer the whole set of $W_{l,fan-out}^i$ as a neuron N_l^i . This neuron receives information from previous layer $l-1$ through its **fan-in** weights $W_{l,fan-in}^i \in \mathbb{R}^{1 \times I_{l-1}}$ (as shown in Fig. 4) and propagates to the next layer through **fan-out** weights $W_{l,fan-out}^i \in \mathbb{R}^{O_l \times 1}$. Also note that $O_{l-1} = I_l$: the output dimension of layer $l-1$ equals to the input dimension of layer l . The weight pixel in layer l at the cross-point of row o and column i is denoted as $W_l^{o,i}$. Moreover, the depth of a DNN model indicates the number of layers it has, and the width refers to the number of filters or neurons of each layer.

c) *Learning units*: Growing or pruning a **filter** W_l^o indicates adding or removing $W_l^o \in \mathbb{R}^{I_l \times K \times K}$ and its corresponding output feature map. Growing or pruning a **neuron** N_l^i means adding or removing both $W_{l,fan-out}^i \in \mathbb{R}^{O_l \times 1}$ and $W_{l,fan-in}^i \in \mathbb{R}^{1 \times I_{l-1}}$.

B. Saliency Score

We adopt a saliency score to measure the effect of a single filter/neuron on the loss function, i.e, the importance of each learning unit. The saliency score is developed from the Taylor Expansion of the loss function. Previously, [37] applied it on pruning. In this paper, we adopt this saliency score and apply it on the growth and pruning scheme. In this section, we provide a mathematical formulation of the saliency score.

The saliency score represents the difference between the loss with and without each unit. In other words, if the removal of a filter/neuron leads to relatively small accuracy degradation, this unit is recognized as an unimportant unit, and vice versa.

Algorithm 1 Entire flow**Input:** Model seed $M_{initial}$

- 1: Initialize a small network model $M_{current} \leftarrow M_{initial}$.
- 2: **for** epoch = 1 to E **do**
- 3: Train current model $M_{current}$ and fetch *Accuracy*.
- 4: **if** $\text{epoch} \% \frac{1}{f_{growth}} = 0$ and $M_{current} < \tau_{capa.}$ **then**
- 5: Grow the network according to Algorithm 2
- 6: $M_{current} \leftarrow M_{grown}$.
- 7: **end if**
- 8: $M_{peak} \leftarrow M_{current}$.
- 9: **if** $\text{epoch} \% \frac{1}{f_{pruning}} = 0$ and $\text{Accuracy} > \tau_{accu.}$ **then**
- 10: Prune the network following Algorithm 3
- 11: $M_{current} \leftarrow M_{pruned}$.
- 12: **end if**
- 13: **end for**
- 14: $M_{final} \leftarrow M_{current}$ and test M_{final} .

Output: Final compact model M_{final}

Thus, the objective function to get the filter with the highest saliency score is formulated as:

$$\underset{W_l^o}{\operatorname{argmin}} |\Delta \mathcal{L}(W_l^o)| \Leftrightarrow \underset{W_l^o}{\operatorname{argmin}} |\mathcal{L}(\mathcal{Y}; \mathcal{X}, \mathcal{W}) - \mathcal{L}(\mathcal{Y}; \mathcal{X}, W_l^o = \mathbf{0})| \quad (1)$$

Using the first-order of the Taylor Expansion:

$$|\mathcal{L}(\mathcal{Y}; \mathcal{X}, \mathcal{W}) - \mathcal{L}(\mathcal{Y}; \mathcal{X}, W_l^o = \mathbf{0})| \text{ at } W_l^o = \mathbf{0} \quad (2)$$

We get:

$$\begin{aligned} |\Delta \mathcal{L}(W_l^o)| &\simeq \left| \frac{\partial \mathcal{L}(\mathcal{Y}; \mathcal{X}, \mathcal{W})}{\partial W_l^o} W_l^o \right| \\ &= \sum_{i=0}^{I_l} \sum_{m=0}^K \sum_{n=0}^K \left| \frac{\partial \mathcal{L}(\mathcal{Y}; \mathcal{X}, \mathcal{W})}{\partial W_l^{o,i,m,n}} W_l^{o,i,m,n} \right| \end{aligned} \quad (3)$$

Similarly, the saliency score of a neuron is derived as:

$$\begin{aligned} |\Delta \mathcal{L}(N_l^i)| &\simeq \left| \frac{\partial \mathcal{L}(\mathcal{Y}; \mathcal{X}, \mathcal{W})}{\partial W_{l,fan-out}^i} W_{l,fan-out}^i \right| \\ &= \sum_{o=0}^{O_l} \left| \frac{\partial \mathcal{L}(\mathcal{Y}; \mathcal{X}, \mathcal{W})}{\partial W_l^{o,i}} W_l^{o,i} \right| \end{aligned} \quad (4)$$

IV. CGAP METHODOLOGY

With the saliency score as the foundation, we develop the entire CGaP flow atop. This section explains the overall flow and the detailed implementation of each step in CGaP.

The CGaP scheme is described in Algorithm 1. Starting from a small network seed, the growth takes place periodically at a frequency of f_{growth} . During each growth, important learning units are chosen and grown at growth ratio β layer by layer from the bottom (input) to top (output), based on the local ranking of the saliency score. The growth phase stops when reaching a capacity threshold $\tau_{capa.}$, followed by several epochs of training on the peak model M_{peak} . When the training accuracy reaches a threshold $\tau_{accu.}$, the pruning phase starts. Pruning is performed layer by layer, from the bottom

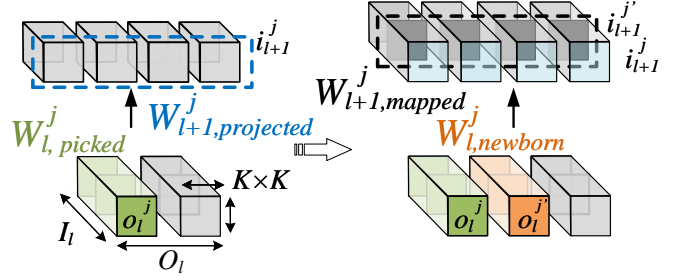


Fig. 3: Illustration of two-step growth in conv-layers. The growth phase follows a two-step (growing and mapping) procedure. After the filter $W_{l,picked}^j$ (green) is picked and split aside, giving birth to $W_{l,newborn}^j$ (orange), the projected input-wise filter, $W_{l+1,projected}^j$ (blue) in layer $l+1$, is as well split aside, generating $W_{l+1,mapped}^j$ (black).

layer to the top layer, at the frequency of $f_{pruning}$. The details in the growth phase and the pruning phase is demonstrated as follows.

A. Growth phase

Algorithm 2 presents the methodology in the growth phase. Each iteration of growth in a layer consists of two steps: growth in layer l and mapping in the adjacent layer. There are two conditions need to be discussed separately: convolutional layers (Fig. 3) and fully-connected layers (Fig. 4). Due to the difference between these two kinds of operation as discussed previously, after the growth of layer l , the mapping in conv-layer takes place at the adjacent layer $l+1$. In fc-layers, the mapping is in layer $l-1$.

a) *Growth in conv-layer l* : According to the local ranking of the saliency score (Eq. 3), we sort all the 3D filters in this layer. With a growth ratio β , $\beta O_{l,t}$ filters are selected in the l -th layer at the t -th growth. On the side of each selected filter $W_{l,picked}^j \in \mathbb{R}^{I_l \times K \times K}$, as shown in Fig. 3. we create a new filter that has the same size, named $W_{l,newborn}^j \in \mathbb{R}^{I_l \times K \times K}$.

In the ideal case, the new filter $W_{l,newborn}^j$ and existing filter $W_{l,picked}^j$ are expected to collaborate with each other and optimize the learning. The existing filter $W_{l,picked}^j$ has already learned on the current task. To keep the same learning pace between the existing filter and the new filter, we initialize $W_{l,newborn}^j$ following:

$$W_{l,newborn}^j = \sigma W_{l,picked}^j + X \sim U([- \mu, \mu]) \quad (5)$$

$$W_{l,picked}^j = \sigma W_{l,picked}^j + X \sim U([- \mu, \mu]) \quad (6)$$

where $\sigma \in (0, 1]$ is a scaling factor and X is a constant following uniform distribution in $[- \mu, \mu]$, where $\mu \in (0, 1]$. Instead of random initialization, the above initialization helps reconcile the learning status of the newborn filters with the old filters. Meanwhile, the scaling factor prevents output from an exponential explosion caused by the feedforward propagation $\mathcal{Y}_l = \mathcal{X}_l * \mathcal{W}_l$. The noise X prevents the learning from sticking at a local minimum that leads to sub-optimal solutions.

Algorithm 2 Growth phase

Input: Current network $M_{current}$

- 1: **for** each layer $l = 1$ to L **do**
- 2: **for** each filter W_l^o in conv-layer l , or each neuron N_l^i in fc-layer l **do**
- 3: Calculate growth score $GS_{W_l^o}$ according to Eq. 3 and $GS_{N_l^i}$ according to Eq. 4.
- 4: **end for**
- 5: Sort all units and select βO_l filters or βI_l neurons with the highest $GS_{W_l^o}$ or $GS_{N_l^i}$.
- 6: **for** each filter $j = 1$ to βO_l (for fc-layer, βI_l) **do**
- 7: Add one filter/neuron on the side of the each picked filter/neuron in layer l .
- 8: Initialize picked and new-born filters (neurons) according to Eq. 5 and Eq. 6.
- 9: Map corresponding input-wise weight in layer $l + 1$ (fan-in weights in layer $l - 1$).
- 10: Initialize projected and mapped filters according to Eq. 7 and Eq. 8 (neurons according to Eq. 9 and Eq. 10).
- 11: **end for**
- 12: **end for**

Output: M_{grown}

Algorithm 3 Pruning phase

Input: Current network $M_{current}$

- 1: **for** each weight $W_l^{o,i,m,n} \in \mathbb{R}^{1 \times 1}$ in conv-layer l or each $W_l^{o,i} \in \mathbb{R}^{1 \times 1}$ in fc-layer l **do**
- 2: Calculate weight pruning score PS_W according to Eq. 11 for conv-layers and Eq. 12 for fc-layers.
- 3: **end for**
- 4: Sort weights by PS_W .
- 5: Zero-out the lowest $\gamma_W \prod[(O_l, I_l, K, K)]$ weights in conv-layer and $\gamma_W \prod[(I_l, O_l)]$ weights in fc-layer.
- 6: **for** each filter W_l^o (neuron N_l^i) in all layers **do**
- 7: Zero-out entire filter W_l^o (neuron N_l^i) if the weight sparsity is larger than pruning rate γ_F (γ_N).
- 8: **end for**

Output: M_{pruned}

b) *Mapping in conv-layer $l + 1$:* After the number of filters in layer l grows from $O_{l,t}$ to $(1 + \beta)O_{l,t}$, the number of output feature map also increases from $O_{l,t}$ to $(1 + \beta)O_{l,t}$. Thus, the input-wise dimension of layer $l + 1$ should increase correspondingly in order to be consistent in data propagation. We implement this by adding a new 4D tensor $W_{l+1,mapped}^j$ adjacent to $W_{l+1,projected}^j$, a projection of $W_{l,picked}^j$ in layer $l + 1$, so that the input dimension increases from $I_{l+1,t}$ to $(1 + \beta)I_{l+1,t}$, where $I_{l+1,t} = O_{l,t}$. The $W_{l+1,mapped}^j$ and $W_{l+1,projected}^j$ are initialized following:

$$W_{l+1,mapped}^j = \sigma W_{l+1,projected}^j + X \sim U([- \mu, \mu]) \quad (7)$$

$$W_{l+1,projected}^j = \sigma W_{l+1,projected}^j + X \sim U([- \mu, \mu]) \quad (8)$$

To summarize, as illustrated in Fig. 3, the filter $W_{l,picked}^j$ (green) is selected according to the saliency score and a new tensor $W_{l,newborn}^j$ (orange) is added. Then the input-wise tensor $W_{l+1,projected}^j$ (in blue dashed rectangular) in layer $l + 1$ is projected, and $W_{l+1,mapped}^j$ (in black dashed rectangular) is generated.

After layer l grows and layer $l + 1$ is mapped, layer $l + 1$ grows and layer $l + 2$ is mapped, so on and so forth till the top convolutional layer. It is worth mentioning that for the ‘projection shortcuts’ [24] with 1×1 convolutions in ResNet [24], the dimension mapping is between the two layers that the shortcut connects to, not necessarily to be the adjacent layers.

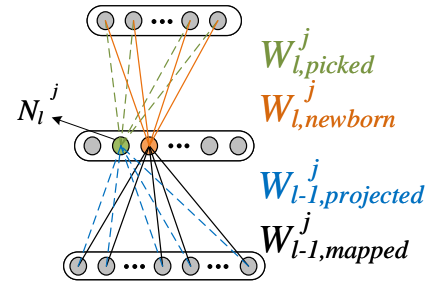


Fig. 4: Illustration of two-step growth in fc-layers. First, fan-out weights $W_{l,newborn}^j$ (orange) is added, then fan-in weights $W_{l-1,mapped}^j$ (black) form the connections from the newborn neuron to all neurons in layer $l - 1$.

c) *Growth and mapping in fc-layers:* As illustrated in Fig. 4, the neuron growth in fc-layers l occurs at fan-out weights, and its initialization follows Eq. 5 and 6.

The mapping in fc-layers take place in the fan-in weights following:

$$W_{l-1,mapped}^j = \sigma W_{l-1,projected}^j + X \sim U([- \mu, \mu]) \quad (9)$$

$$W_{l-1,projected}^j = \sigma W_{l-1,projected}^j + X \sim U([- \mu, \mu]) \quad (10)$$

After growing the last conv-layer, We flatten the output feature map of this conv-layer, treat it as the input from layer $l - 1$ and map in the same manner.

B. Pruning phase

Pruning in each layer consists of two steps: weight pruning and unit pruning. First, we sort weight pixels locally in each conv-layer according to Eq.11:

$$PS_{W_l^{o,i,m,n}} = \left| \frac{\partial \mathcal{L}(\mathcal{Y}; \mathcal{X}, \mathcal{W})}{\partial W_l^{o,i,m,n}} W_l^{o,i,m,n} \right| \quad (11)$$

and in each fc-layer according to Eq.12:

$$PS_{W_l^{o,i}} = \left| \frac{\partial \mathcal{L}(\mathcal{Y}; \mathcal{X}, \mathcal{W})}{\partial W_l^{o,i}} W_l^{o,i} \right| \quad (12)$$

In each layer, $100\gamma_W\%$ weight pixels with the lowest PS_W are set as zero, where $\gamma_W \in (0, 1)$ is the weight pruning rate. Then the entire filter/neuron whose sparsity is larger than the filter/neuron pruning rate γ_F or $\gamma_N \in (0, 1)$ is set to zero. In this way, a large amount of entire filters/neurons are pruned, leading to a compact inference model.

V. ALGORITHMIC EXPERIMENTS

To evaluate the proposed approach, we present experimental results in this section. We perform experiments on several modern DNN structures (LeNet [9], VGG-Net [6], ResNet [24]) and representative datasets (MNIST [9], CIFAR-10, CIFAR-100 [27], SVHN [23]).

A. Training Setup

a) Network structures: The LeNet-5 architecture consists of two sets of convolutional, ReLU [38] and max pooling layers, followed by two fully-connected layers and finally a softmax classifier. The VGG-16 and VGG-19 structures we use have the same convolutional structure as [6] but are redesigned with only two fully-connected to be fairly compared with the pruning-only method [14]. Therefore, the VGG-16 (VGG-19) has 13 (16) convolutional layers, each is followed by a batch normalization layer [39] and a ReLU activation. The structures of ResNet-56 and ResNet-110 follow [14]. Each convolutional layer (except skip-connections) is followed by a batch normalization layer and ReLU activation. During the training, the depth of the networks remains constant since CGaP does not touch the depth of the network, but the width of each layer changes.

Note that in the following text, we denote the full-size models trained from scratch without sparsity regularization as ‘baseline’. The three-step pruning schemes that remove weights or filters but do not execute network growth are denoted as ‘pruning-only’ models.

b) Datasets: MNIST is a handwritten digit dataset in grey-scale (i.e., one color channel) with 10 classes from digit 0 to digit 9. It consists of 60,000 training images and 10,000 testing images. The CIFAR-10 dataset consists of 60,000 32×32 color images in 10 classes, with 5000 training images and 1000 testing images per class. The CIFAR-100 dataset has 100 classes, including 500 training images and 100 testing images per class. The Street View House Number (SVHN) is a real-world color image dataset that is resized to a fixed resolution of 32×32 pixels. It contains 73,257 training images and 26,032 testing images.

TABLE I: Evaluation of the performance on MNIST.

Method	Accuracy	FLOPs	Pruned	Param.	Pruned
LeNet5-Baseline	99.29	4.59M	–	431K	–
Pruning [15]	99.26	0.85M	81.5%	112K	74.0%
Pruning [13]	99.23	0.73M	84.0%	36K	92.0%
CGaP	99.36	0.44M	90.4%	8K	98.1%

TABLE II: Evaluation of the performance on CIFAR-100. ‘NA’ means ‘not available’ in the original paper.

Method	Accuracy	FLOPs	Pruned	Param.	Pruned
VGG19-Baseline	72.63	797M	–	20.4M	–
Pruning [25]	71.85	NA	–	10.1M	50.5%
Pruning [16]	72.85	501M	37.1%	5.0M	75.5%
CGaP	73.00	373M	53.2%	4.3M	78.9%

TABLE III: Evaluation of the performance on SVHN.

Method	Accuracy	FLOPs	Pruned	Param.	Pruned
VGG19-Baseline	96.02	797M	–	20.4M	–
Pruning [16]	96.13	398M	50.1%	3.1M	84.8%
CGaP	96.25	206M	74.2%	2.9M	85.8%

TABLE IV: Evaluation of the performance on CIFAR-10.

Method	Accuracy	FLOPs	Pruned	Param.	Pruned
VGG16-Baseline	93.25	630M	–	15.3M	–
Pruning [14]	93.40	410M	34.9%	5.4M	64.7%
CGaP	93.59	280M	56.2%	4.5M	70.6%
ResNet-56-Baseline	93.03	268M	–	0.85M	–
Pruning [25]	92.56	182M	32.1%	0.73M	14.1%
CGaP	93.20	181M	32.5%	0.53M	37.6%
ResNet-110-Baseline	93.34	523M	–	1.72M	–
Pruning [14]	93.11	310M	40.7%	1.16M	32.6%
Pruning [26]	93.52	300M	40.8%	NA	–
CGaP	93.43	192M	63.3%	0.62M	64.0%

c) Hyper-parameters: We set the learning rate to be 0.1 and divide by 10 for every 30% of the training epochs. We train our model using Stochastic Gradient Descent (SGD) with a batch size of 128 examples, a momentum of 0.9, and a weight decay of 0.0005. The loss function is the cross-entropy loss with softmax function. We train 60, 200, 220 and 100 epochs on MNIST, CIFAR-10, CIFAR-100 and SVHN datasets, respectively. In the growth phase, we have hyper-parameters set as follows: the growth stopping condition $\tau_{capa.} = O_{1,baseline}$, i.e., the growth stops at the t -th growth if the number of filters in the $(t+1)$ -th growth is larger than the baseline model. The growth ratio β is set as 0.6. The growth frequency f_{growth} is set as $1/3$. The scaling factor σ in Eq. 5 to Eq. 10 is set to 0.5 and μ is 0.1. The pruning frequency $f_{pruning}$ is set to be 1. The setting of the weight pruning rate γ_W follows [13], [14] and [16] for LeNet-5, VGG-Net and ResNet, respectively. γ_F and γ_N is set to be same as γ_W .

d) Framework and platform: The experiments are performed with PyTorch [40] framework on one NVIDIA GeForce GTX 1080 Ti platform. It is worth mentioning that experiments performed with different frameworks may have variation in accuracy and performance. Thus, to have a fair comparison among CGaP, baseline and pruning-only methods, all the data are performed with PyTorch framework.

B. Performance Evaluation

With training setup as aforementioned, we perform experiments on several datasets with modern DNN architectures. In Table I, Table II, Table III and Table IV, we summarize

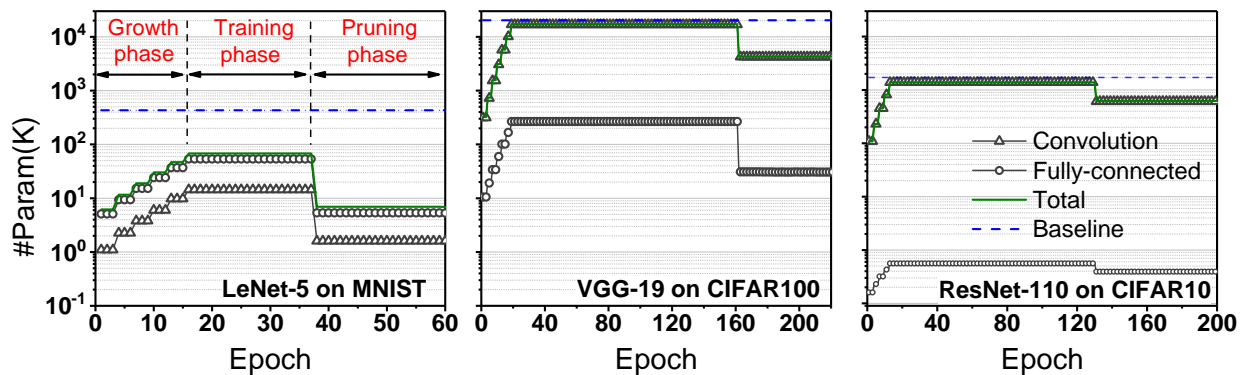


Fig. 5: Number of parameters during training, plotted at the end of each epoch. In the beginning, the model size increases gradually due to the growth. After the growth ends and several epochs of training on the peak model, one drop can be observed after the first pruning. There are several iterations of pruning at a frequency of 1.

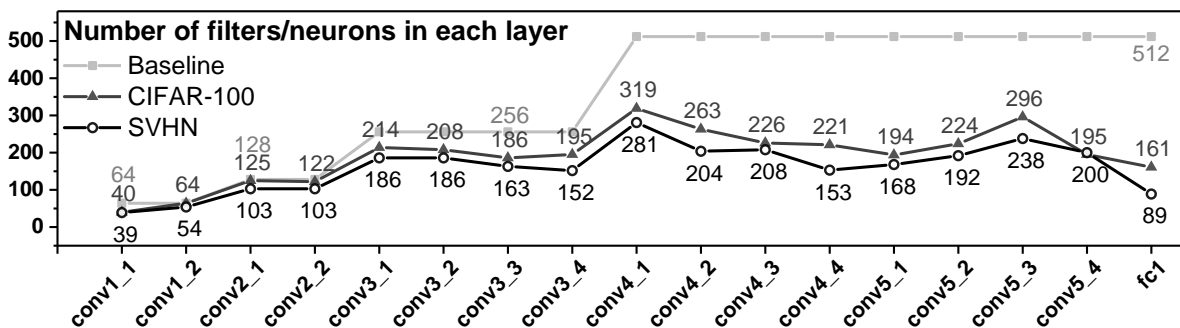


Fig. 6: The VGG-19 structures learned by CGaP on CIFAR-100 and SVHN datasets. The shared Y-axis for three sub-./ is the number of parameters of the model.

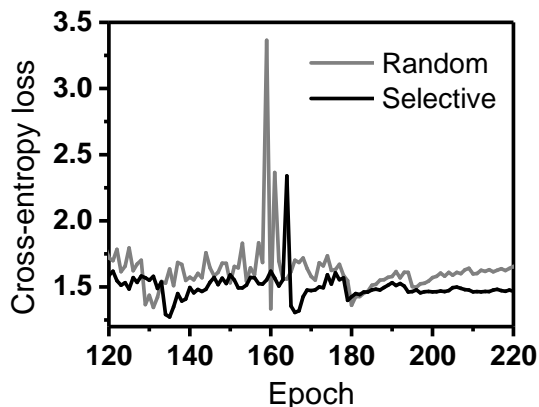


Fig. 7: Saliency-based growth outperforms random growth. The loss is monotonically decreasing from epoch 0 to 220 with small glitches. Here we zoomed in from epoch 120 to 220 to show the loss at the end of the training.

the performance attained by CGaP on MNIST, CIFAR-100, SVHN, and CIFAR-10 datasets, respectively. To be specific, the second column ‘Accuracy’ denotes the inference accuracy in percentage achieved by the baseline model, the up-to-date pruning-only approaches and CGaP approach, respectively. The column ‘FLOPs’ represent the calculated number of FLOPs of a single inference pass. The calculation of FLOPs

follows the method described in [37]. Fewer FLOPs means lower computation cost in one inference pass. The neighboring column ‘Pruned’ represents the reduction of FLOPs in the compressed model as compared to the baseline model. The column ‘Param.’ stands for the number of parameters of the inference model. Fewer parameters promise a smaller model size. The last column ‘Prunes’ denotes the percentage pruned in parameters compared to the baseline. Larger pruned percentage implies fewer computation operations and more compact model. The best result of each column is highlighted in bold.

The results shown in Table I to IV prove that CGaP outperforms the previous pruning-only approaches in accuracy and model size. For instance, as displayed in Table IV, on ResNet-56, our CGaP approach achieves 93.20% accuracy with 32.5% reduction in FLOPs and 37.6% reduction in parameters, while the up-to-date pruning-only method [25] that deals with static structure only reaches 92.56% accuracy with 32.1% reduction in FLOPs and 14.1% reduction in parameters. On ResNet-110, though [26] achieves 0.09% higher accuracy than CGaP, CGaP overwhelms it by trimming 22.5% more FLOPs.

C. Visualization of the dynamic structures

Fig. 5 presents the dynamic model size during CGaP training. During the growth phase, the model size continuously increases and reaches a peak capacity. When the pruning phase starts, the model size drops.

Furthermore, the sparsity achieved by CGaP is structured. In other words, a large amount of filters and neurons are entirely pruned. For instance, the baseline LeNet-5 without sparsity regularization has 20, 50 filters in conv-layer 1 and conv-layer 2, 500 and 10 neurons in fc-layer 1 and fc-layer 2, denoted as [20-50-500-10] (number of filters/neurons in [conv1-conv2-fc1-fc2]). The model achieved by CGaP contains only 8, 17 filters and 23, 10 neurons, denoted as [8-17-23-10]. Compared to baseline results, CGaP significantly decreases 60%, 66%, 95.4% units for each layer (the output layer should remain the same as the number of classes all the time). In this case, the pruned filters and neurons are skipped in the inference pass and thus accelerating the computation pipeline on hardware.

Another example is provided in Fig. 6. Fig. 6 visualizes the VGG-19 structures from CGaP as well as the baseline structure on two different tasks. In the baseline model, the width (number of filters/neurons) of each layer is abundant, from 64 filters (the bottom conv-layers) to 512 filters (the top conv-layers). The baseline VGG-19 structure is designed to have a large enough size in order to guarantee the learning capacity. However, it turns out to be redundant, as proved by the structure that CGaP generated: 37.7% to 82.6% filters are pruned out in each layer. Meanwhile, in the baseline mode, the top conv-layers are designed to have more filters than the bottom layers, but CGaP shows that it is not always necessary for top layers to have a relatively large size.

D. Validating the saliency-based growth

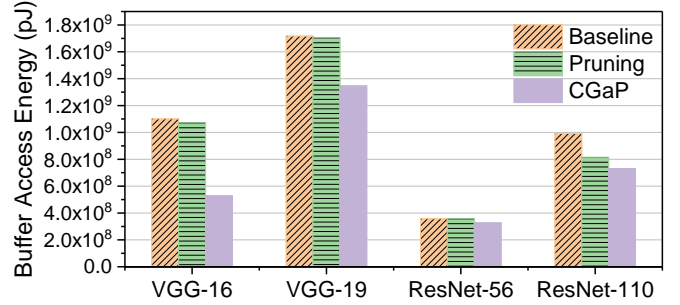
Fig. 7 validates the efficacy of our saliency-based growth policy. Selective growth, which emphasizes on the important units according to the saliency score, has lower cross-entropy loss than randomly growing some units. The spiking in Fig. 7 is caused by the first iteration of pruning and this loss is recovered by the following iterative fine-tuning. In selective growth, this loss is $1.4\times$ lower than that in random growth. This phenomenon supports our argument that selective growth assists the pruning phase. The detailed understanding of growth will be further discussed in Section VII.

To summarize the results from the algorithm simulations, the proposed CGaP approach:

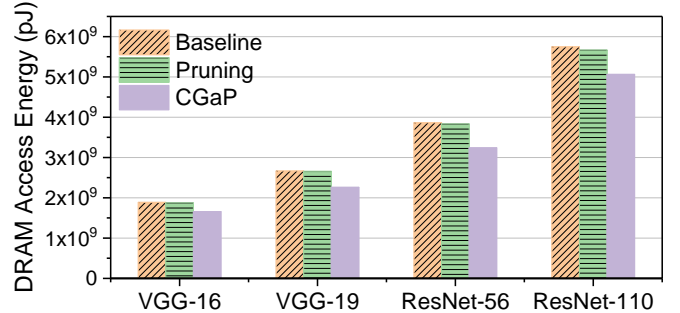
- Largely compresses the model size by 37.6% to 98.1% on representative DNN structures.
- Decreases the inference cost, to be specific, number of FLOPs, by 32.5% to 90.4% on various datasets.
- Does not sacrifice accuracy and even improves accuracy.
- Outperforms the state-of-the-art pruning-only methods that deal with fixed structures.

VI. EXPERIMENTS ON FPGA SIMULATOR

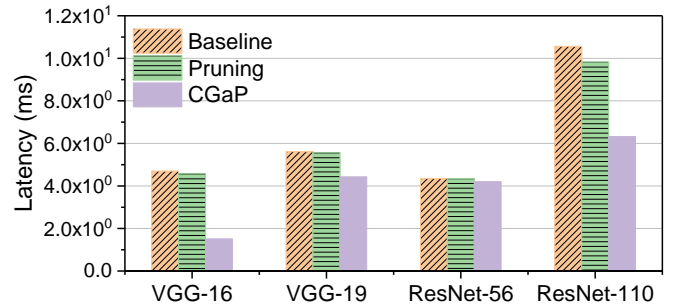
The results above demonstrate that CGaP generates an accurate and small inference model. In this section, we further evaluate the on-chip inference cost of the generated models and compare CGaP with previous non-structured pruning [13]. As CGaP achieves structured sparsity, it is expected CGaP outperforms the previous non-structured pruning in hardware acceleration and power efficiency. To validate, we perform the estimation of buffer access energy, DRAM access energy and latency using the performance model of FPGA [5].



(a) Comparison of three schemes in buffer access energy (pJ) for VGG-16 on CIFAR-10, VGG-19 on CIFAR-100, ResNet-56 and ResNet-110 on CIFAR-10.



(b) Comparison of three schemes in DRAM access energy (pJ) for VGG-16 on CIFAR-10, VGG-19 on CIFAR-100, ResNet-56 and ResNet-110 on CIFAR-10.



(c) Comparison of three schemes in on-chip inference latency (ms) for VGG-16 on CIFAR-10, VGG-19 on CIFAR-100, ResNet-56 and ResNet-110 on CIFAR-10.

Fig. 8: Estimation on FPGA performance model.

A. Overview of the FPGA simulator

[5] is a high-level performance model designed to estimate the number of external and on-chip memory access, as well as the latency. The resource costs are formulated by the acceleration strategy as well as the design variables that control the loop tiling and unrolling. The performance model has been validated across several modern DNN algorithms in comparison to on-board testings on two FPGAs, with the differences within 3%.

In the following experiments, the setup follows: the pixels and weights are both 16-bit fixed point, the data width of DRAM controller is 512 bits, the accelerator operating frequency is 300 MHz, and the DRAM bandwidth is 19.2 GB/second. The parameters related to loop tiling and unrolling follow the setting in [5].

B. Results from FPGA performance model

The on-chip and external memory access energy across VGG-16, VGG-19, ResNet-56 and ResNet-110 is displayed in Fig. 8(a) and Fig. 8(b), respectively. The inference latency is shown in Fig. 8(c). Though the models generated from weight magnitude pruning and CGaP have the same sparsity, CGaP outperforms non-structured magnitude weight pruning in hardware efficiency and acceleration. For example, with the same setup of the pruning ratio during training, magnitude weight pruning decreases 1.0% on-chip access energy, 1.0% DRAM access energy and 0.8% latency for VGG-19 on CIFAR-100, while the CGaP achieves 21.6%, 15%, and 21.1% reduction. The non-structured weight pruning [13] is able to improve the power and latency efficiency in comparison to baseline, however, the improvement is limited. In contrast, CGaP achieves significant acceleration and energy reduction. The reason is that the non-structured sparsity, i.e., scattered weight distribution, leads to irregular memory access that weakens the acceleration on hardware in a real scenario.

VII. DISCUSSION

In Section V and VI, the performance of CGaP has been comprehensively evaluated on algorithm platforms and hardware platforms. In this section, we provide a more in-depth understanding of the growth to explain why selective growth is able to improve the performance from the traditional pipelines. Furthermore, we provide a thorough ablation study to validate the robustness of the proposed CGaP method.

a) Understanding the growth: Fig. 9 illustrates a visualization of the weights in the bottom conv-layer (conv1_1) in VGG-19, at the moment of initialization, after the first growth, after the last growth and when training ends. Inside each figure, the upper bar is the CGaP model, whose size varies at different training moments. The lower bar is from the baseline model, whose size is static during training. At the initialization moment (Fig. 9(a)), CGaP model only has 8 filters in this layer while the baseline model has 64 filters. Then the number of filters grows to 13 after one iteration growth (Fig. 9(b)), meaning the most important 5 filters are selected and added. It is clear that the pattern in Fig. 9(b) is more active than that in (a), indicating the filters have already fetched effective features from the input images. More important, along with the growing, the pattern in CGaP model becomes more structured than that in the baseline model, as shown in Fig. 9(c). Benefiting from this well-structured pattern, our CGaP model has higher learning accuracy than the baseline model. From Fig. 9(c) to Fig. 9(d), relatively unimportant filters are removed, and important ones are kept. We observe that most of the filters that are favored by the growth, such as filters at index 36, 48, 72, 96 in Fig. 9(c), are still labeled as important filters in Fig. 9(d) even after a long training process between the growth phase and the pruning phase. Leveraging the growth policy, the model is able to recover quickly from the loss caused by pruning (the spiking in Fig. 7).

b) Robustness of the seed: The performance of CGaP is stable under the variation of the initial seeds. To prove this, we

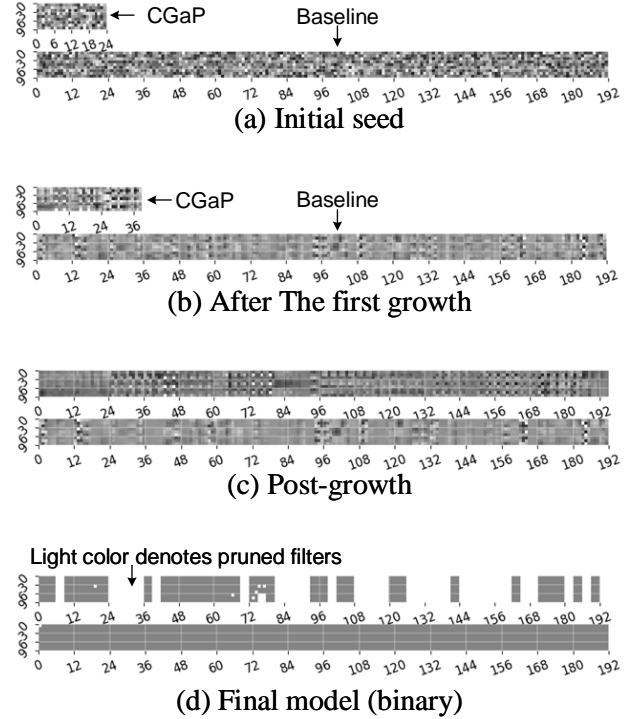


Fig. 9: Visualization of the filters in conv1_1 in VGG-19 on CIFAR-100 at four specific moments (a-d). Inside each figure, the top bar is CGaP model and the bottom bar is baseline model. X-axis is the index of output-wise weights and Y-axis is the index of input-wise weights.

scan several seeds in different size and present the variation in accuracy and inference model size. The structure of 6 scanned seeds is listed in Table V. Each seed has a different number of filters in each layer, e.g., seed ‘2’ has 2 filters in block conv1. The size of the seeds varies from 0.01M to 0.53M. Fig. 10 presents the final model size and the number of growth of each seed. A larger seed leads to a larger final model but requires fewer iterations of growth to reach the intended model size. Generally speaking, there is a trade-off between the inference accuracy and the model size. Though the seed varies a lot from each other, the final accuracy is quite robust, as listed in the ‘Accuracy’ row in Table V. It is worth mentioning that, even though the seed ‘2’ degrades the accuracy of 0.69% from baseline, the inference model size is only 2.4M, significantly smaller than 20.4M, the baseline size.

c) Robustness of the hyper-parameters: CGaP is conditioned on a set of hyper-parameters to achieve an optimal performance, while it is stable under the variation of these hyper-parameters. Empirically, we leverage the following experience to perform parameter optimization: a smaller growth rate β for a larger seed and vice versa; threshold τ_{capa} is set based on the user’s intended model size; a smaller f_{growth} for a complicated dataset and vice versa; a relatively greedy growth (larger β and f_{growth}) prefers a larger noise μ but smaller σ to push the model away from sticking at a local

Initial seeds		'2'	'4'	'6'	'8'	'10'	'12'
#filters	conv1_n	2	4	6	8	10	12
	conv2_n	4	8	12	16	20	24
	conv3_n	8	16	24	32	40	48
	conv4_n	16	32	48	64	80	96
	conv5_n	16	32	48	64	80	96
#param	Initial (M)	0.01	0.06	0.13	0.23	0.36	0.53
Testing accuracy*		-0.69%	-0.2%	-0.16%	+0.37%	+0.04%	0.29%
*Relative accuracy of the final VGG-19 model on CIFAR-100 as compared to the baseline.							

TABLE V: The impact of various structures and sizes of the initial seed of VGG-19.

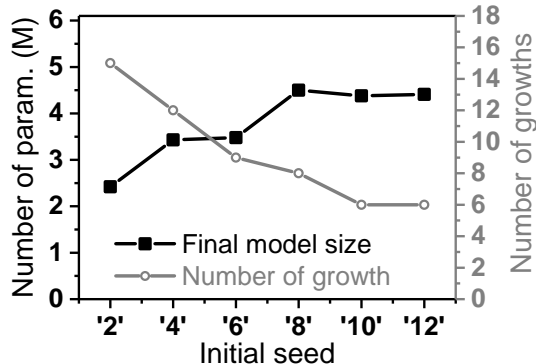


Fig. 10: A larger seed leads to a larger final model but fewer iterations in the growth phase.

minimum. Tuning of the pruning ratio in each layer is in a similar manner to the other pruning works [13] [14].

In particular, we scan 121 combinations of the scaling factor σ and noise μ in the range $[0.0, 1.0]$ with the step=0.1 and provide the following discussion. For VGG16 on CIFAR-10, the accuracy of several corner cases are 90% ($\mu=1, \sigma=0$, which is a case of random initialization), 89% ($\mu=1, \sigma=1$), 84% ($\mu=0, \sigma=1$, which is another case of mimicking its neighbor without scaling) and 10% ($\mu=0, \sigma=0$, the training is invalid in this case), 93% ($\mu=0, \sigma=0$, which is another case of mimicking its neighbor with scaling), 88% ($\mu=0.5, \sigma=0$, which is another case of random initialization). The best accuracy of 93.6% is under $\mu=0.1, \sigma=0.5$. The combinations in the zone that $\mu \in [0, 0.5]$ and $\sigma \in (0, 0.5]$ always provide $>92\%$ accuracy. To summarize, σ impacts more than μ as μ is relatively small; σ should not be too large and 0.5 is safe for future tasks and networks; adding a noise improves the accuracy (like from 93% to 93.6%) as it prevents local minimum; inheriting from the neighbor is more efficient than randomly initializing since the network is able to resume the learning right after the growth.

VIII. CONCLUSION AND FUTURE WORK

Modern DNNs typically start training from a fixed and over-parameterized network, which leads to redundancy and is lack of structural plasticity. We propose a novel dynamic training algorithm, Continuous Growth and Pruning, that initializes training from a small network, expands the network width continuously to learn important learning units and structures,

and finally prunes secondary ones. The effectiveness of CGaP depends on where to start and stop the growth, which learning unit (filter and neuron) should be added, and how to initialize the newborn units to ensure model convergence. Our experiments on benchmark datasets and architectures demonstrate the advantage of CGaP on learning efficiency (accurate and compact). We further validate the energy and latency efficiency of the inference model generated by CGaP on FPGA performance simulator. Our approach and analysis will help shed light on the development of adaptive neural networks for dynamic tasks such as continual and lifelong learning.

ACKNOWLEDGMENT

This work was supported in part by C-BRIC, one of six centers in JUMP, a Semiconductor Research Corporation (SRC) program sponsored by DARPA. It was also partially supported by National Science Foundation (NSF) under CCF #1715443.

REFERENCES

- [1] A. Krizhevsky, I. Sutskever, and G. E. Hinton, "Imagenet classification with deep convolutional neural networks," in *Advances in neural information processing systems*, pp. 1097–1105, 2012.
- [2] S. Ren, K. He, R. Girshick, and J. Sun, "Faster r-cnn: Towards real-time object detection with region proposal networks," in *Advances in Neural Information Processing Systems*, pp. 91–99, 2015.
- [3] A. Graves, A.-r. Mohamed, and G. Hinton, "Speech recognition with deep recurrent neural networks," in *Acoustics, Speech and Signal Processing (ICASSP), 2013 IEEE International Conference on*, pp. 6645–6649, IEEE, 2013.
- [4] P. Zhang, Y. Goyal, D. Summers-Stay, D. Batra, and D. Parikh, "Yin and yang: Balancing and answering binary visual questions," in *Proceedings of the IEEE Conference on Computer Vision and Pattern Recognition*, pp. 5014–5022, 2016.
- [5] Y. Ma, Y. Cao, S. Vrudhula, and J.-s. Seo, "Performance modeling for cnn inference accelerators on fpga," *IEEE Transactions on Computer-Aided Design of Integrated Circuits and Systems*, 2019.
- [6] K. Simonyan and A. Zisserman, "Very deep convolutional networks for large-scale image recognition," *arXiv preprint arXiv:1409.1556*, 2014.
- [7] Y. Chen, T. Luo, S. Liu, S. Zhang, L. He, J. Wang, L. Li, T. Chen, Z. Xu, N. Sun, *et al.*, "Dadiannao: A machine-learning supercomputer," in *Proceedings of the 47th Annual IEEE/ACM International Symposium on Microarchitecture*, pp. 609–622, IEEE Computer Society, 2014.
- [8] Z. Du, R. Fasthuber, T. Chen, P. Ienne, L. Li, T. Luo, X. Feng, Y. Chen, and O. Temam, "Shidiannao: Shifting vision processing closer to the sensor," in *ACM SIGARCH Computer Architecture News*, vol. 43, pp. 92–104, ACM, 2015.
- [9] Y. LeCun, L. Bottou, Y. Bengio, P. Haffner, *et al.*, "Gradient-based learning applied to document recognition," *Proceedings of the IEEE*, vol. 86, no. 11, pp. 2278–2324, 1998.

- [10] A. Shafiee, A. Nag, N. Muralimanohar, R. Balasubramonian, J. P. Strachan, M. Hu, R. S. Williams, and V. Srikumar, "Isaac: A convolutional neural network accelerator with in-situ analog arithmetic in crossbars," *ACM SIGARCH Computer Architecture News*, vol. 44, no. 3, pp. 14–26, 2016.
- [11] J. Qiu, J. Wang, S. Yao, K. Guo, B. Li, E. Zhou, J. Yu, T. Tang, N. Xu, S. Song, *et al.*, "Going deeper with embedded fpga platform for convolutional neural network," in *Proceedings of the 2016 ACM/SIGDA International Symposium on Field-Programmable Gate Arrays*, pp. 26–35, ACM, 2016.
- [12] C. Farabet, C. Poulet, J. Y. Han, and Y. LeCun, "Cnp: An fpga-based processor for convolutional networks," in *2009 International Conference on Field Programmable Logic and Applications*, pp. 32–37, IEEE, 2009.
- [13] S. Han, J. Pool, J. Tran, and W. Dally, "Learning both weights and connections for efficient neural network," in *Advances in Neural Information Processing Systems*, pp. 1135–1143, 2015.
- [14] H. Li, A. Kadav, I. Durdanovic, H. Samet, and H. P. Graf, "Pruning filters for efficient convnets," *arXiv preprint arXiv:1608.08710*, 2016.
- [15] H. Hu, R. Peng, Y.-W. Tai, and C.-K. Tang, "Network trimming: A data-driven neuron pruning approach towards efficient deep architectures," *arXiv preprint arXiv:1607.03250*, 2016.
- [16] Z. Liu, J. Li, Z. Shen, G. Huang, S. Yan, and C. Zhang, "Learning efficient convolutional networks through network slimming," in *Proceedings of the IEEE International Conference on Computer Vision*, pp. 2736–2744, 2017.
- [17] J.-H. Luo, J. Wu, and W. Lin, "Thinet: A filter level pruning method for deep neural network compression," in *Proceedings of the IEEE international conference on computer vision*, pp. 5058–5066, 2017.
- [18] V. Lebedev and V. Lempitsky, "Fast convnets using group-wise brain damage," in *2016 IEEE Conference on Computer Vision and Pattern Recognition (CVPR)*, pp. 2554–2564, IEEE, 2016.
- [19] W. Wen, C. Wu, Y. Wang, Y. Chen, and H. Li, "Learning structured sparsity in deep neural networks," in *Advances in Neural Information Processing Systems*, pp. 2074–2082, 2016.
- [20] J. H. Gilmore, W. Lin, M. W. Prastawa, C. B. Looney, Y. S. K. Vetsa, R. C. Knickmeyer, D. D. Evans, J. K. Smith, R. M. Hamer, J. A. Lieberman, *et al.*, "Regional gray matter growth, sexual dimorphism, and cerebral asymmetry in the neonatal brain," *Journal of Neuroscience*, vol. 27, no. 6, pp. 1255–1260, 2007.
- [21] S. J. Lipina and J. A. Colombo, *Poverty and brain development during childhood: An approach from cognitive psychology and neuroscience*. American Psychological Association, 2009.
- [22] M. Butz and A. van Ooyen, "A simple rule for dendritic spine and axonal bouton formation can account for cortical reorganization after focal retinal lesions," *PLoS computational biology*, vol. 9, no. 10, p. e1003259, 2013.
- [23] Y. Netzer, T. Wang, A. Coates, A. Bissacco, B. Wu, and A. Y. Ng, "Reading digits in natural images with unsupervised feature learning," 2011.
- [24] K. He, X. Zhang, S. Ren, and J. Sun, "Deep residual learning for image recognition," in *Proceedings of the IEEE conference on computer vision and pattern recognition*, pp. 770–778, 2016.
- [25] Z. Liu, M. Sun, T. Zhou, G. Huang, and T. Darrell, "Rethinking the value of network pruning," *arXiv preprint arXiv:1810.05270*, 2018.
- [26] Y. He, G. Kang, X. Dong, Y. Fu, and Y. Yang, "Soft filter pruning for accelerating deep convolutional neural networks," *arXiv preprint arXiv:1808.06866*, 2018.
- [27] A. Krizhevsky and G. Hinton, "Learning multiple layers of features from tiny images," tech. rep., Citeseer, 2009.
- [28] S. Han, X. Liu, H. Mao, J. Pu, A. Pedram, M. A. Horowitz, and W. J. Dally, "Eie: efficient inference engine on compressed deep neural network," in *Computer Architecture (ISCA), 2016 ACM/IEEE 43rd Annual International Symposium on*, pp. 243–254, IEEE, 2016.
- [29] B. Liu, M. Wang, H. Foroosh, M. Tappen, and M. Pensky, "Sparse convolutional neural networks," in *Proceedings of the IEEE Conference on Computer Vision and Pattern Recognition*, pp. 806–814, 2015.
- [30] T. Ash, "Dynamic node creation in backpropagation networks," *Connection science*, vol. 1, no. 4, pp. 365–375, 1989.
- [31] B. Bredis and T. Gedeon, "Using the grow-and-prune network to solve problems of large dimensionality," 1998.
- [32] X. Dai, H. Yin, and N. K. Jha, "Nest: A neural network synthesis tool based on a grow-and-prune paradigm," *arXiv preprint arXiv:1711.02017*, 2017.
- [33] Y. Gong, L. Liu, M. Yang, and L. Bourdev, "Compressing deep convolutional networks using vector quantization," *arXiv preprint arXiv:1412.6115*, 2014.
- [34] I. Hubara, M. Courbariaux, D. Soudry, R. El-Yaniv, and Y. Bengio, "Quantized neural networks: Training neural networks with low precision weights and activations," *The Journal of Machine Learning Research*, vol. 18, no. 1, pp. 6869–6898, 2017.
- [35] E. L. Denton, W. Zaremba, J. Bruna, Y. LeCun, and R. Fergus, "Exploiting linear structure within convolutional networks for efficient evaluation," in *Advances in neural information processing systems*, pp. 1269–1277, 2014.
- [36] C. Leng, Z. Dou, H. Li, S. Zhu, and R. Jin, "Extremely low bit neural network: Squeeze the last bit out with admm," in *Thirty-Second AAAI Conference on Artificial Intelligence*, 2018.
- [37] P. Molchanov, S. Tyree, T. Karras, T. Aila, and J. Kautz, "Pruning convolutional neural networks for resource efficient inference," *arXiv preprint arXiv:1611.06440*, 2016.
- [38] V. Nair and G. E. Hinton, "Rectified linear units improve restricted boltzmann machines," in *Proceedings of the 27th international conference on machine learning (ICML-10)*, pp. 807–814, 2010.
- [39] S. Ioffe and C. Szegedy, "Batch normalization: Accelerating deep network training by reducing internal covariate shift," *arXiv preprint arXiv:1502.03167*, 2015.
- [40] A. Paszke, S. Gross, S. Chintala, G. Chanan, E. Yang, Z. DeVito, Z. Lin, A. Desmaison, L. Antiga, and A. Lerer, "Automatic differentiation in pytorch," 2017.